# Modeling and Experimental Work on Electrical Discharge Machining

**Panagiotis Karmiris-Obratański, Emmanouil L. Papazoglou, and Angelos P. Markopoulos**

**Abstract** Electrical Discharge Machining (EDM) is a non-conventional machining process, widely utilized in the modern industrial environment, especially in applications that involve the manufacturing of complex shapes and geometries, along with high dimensional accuracy. Conceptually EDM is a simple process, which is based on the erosion that accompanies the spark occurrence between two electrically conductive materials, one that acts as working electrode and one as the workpiece. Nevertheless, in practice, and due to the technological advances in the relevant field, EDM has become a multi-parameter machining process. The current chapter aims to familiarize the reader with the process of EDM, while at the same time, to provide useful and practical information concerning more advanced topics. The chapter's first sections are an introduction to the EDM, where a brief historical review, and the basic working principles are presented. The basic physical mechanisms that take place during machining are analyzed, along with the major machining parameters and performance indexes. Moreover, a brief literature review concerning the machining of steel and aluminum alloys with EDM is quoted. Thereafter, the basic principles for modeling and simulation of the process are introduced, aiming to become a helpful reference in model development. Finally, in the last section, a comparative study regarding the machining of two different aluminum alloys (i.e., Al5052 and Al6063) with EDM is presented, indicating how different alloys of the same base may have different behavior during their machining with EDM.

P. Karmiris-Obratański · E. L. Papazoglou · A. P. Markopoulos (✉)
School of Mechanical Engineering - Laboratory of Manufacturing Technology,
National Technical University of Athens, Athens, Greece
e-mail: amark@mail.ntua.gr

P. Karmiris-Obratański
Faculty of Mechanical Engineering and Robotics - Department of Manufacturing Systems,
AGH University of Science and Technology, Cracow, Poland

# 1 A Brief History of EDM

Electrical discharge machining (EDM) is one of the most extensively used non-conventional machining processes, with many applications in the modern industrial environment. The main advantage of EDM is the capability of machining any electrically conductive material, regardless of its mechanical properties, e.g. strength and hardness, in complex geometries and with high dimensional accuracy. EDM finds a wide range of applications in the fields of die and mold manufacturing, aerospace, automotive industries, microelectronics, and biomedical engineering [1, 2]. The original idea of this process came during the eighteenth century when scientist Benjamin Franklin reported the erosion phenomenon of metal workpieces by electrical sparks [3]. About 70 years later the scientist Joseph Priestly discovered the erosive effect of electrical discharges.

A couple of Russian scientists, namely Dr Boris Lazarenko and his wife, Dr Natalia Lazarenko (Fig. 1) were asked to develop a solution for tungsten contact points in the military vehicles distributors to avoid erosion due to friction. At these contacts, occurred small discharges that affected the surface quality of the contact points, and small craters appeared due to the material erosion phenomenon. They discovered that mineral oils could make the sparks more predictable and uniform. These uniform sparks led to more uniform erosion phenomena on the tungsten surface, which was one of the hardest known material at these times. Immediately the Lazarenko couple realized the potential of their discovery, and they decided to create the first.

EDM prototype for industrial machining purposes, they also published their thesis entitled "Investigation of the Effect of Wear on Electric Power Contacts for Manufacturing Purposes" [4]. The following Fig. 1. shows the schematic structure of their EDM prototype which is similar schematic structure to the spark distribution unit.

At the early 1940s was invented the die-sinking EDM process with the advent of pulse generators planetary and orbital motion techniques, CNC and the adaptive control mechanism. So the EDM machine process was in commercial use in 1952 by the "Charmilles" industry which was presented for the first time as the European Machine Tool Exhibition in 1955 [5], and in 1972 "Agie" another company
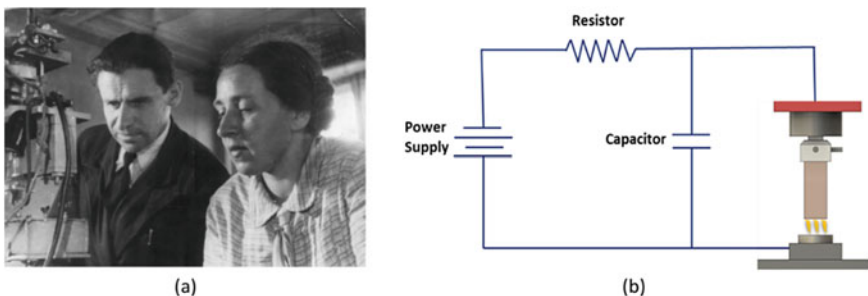


**Fig. 1** On the left side **a** Dr. Boris and Dr. Natalia Lazarenko working on their EDM prototype, and on the right side **b** is the schematic representation of their machine

was invented the wire-ED machining process that included powerful generators, improved machine intelligence, better flushing solution and new wire electrodes [6]. "Seibu" developed the first CNC wire EDM machine in 1972 and the first system was manufactured in Japan. Kurafuii and Masuzawa in 1968 demonstrated the development of the first micro- EDM machining process when they drilled a minute hole in a 50 μm thick carbide plate.

## 2 Introduction and Basic Theory of EDM

The development of modern technology is determined in many respects by new materials difficult to process by conventional methods. Their commercialization and application in industrial conditions involve the development of appropriate machining technologies. One of the modern methods that makes it possible to shape conductive materials, regardless of their hardness, as well as the chemical composition, is electro erosive machining. An unconventional method of material removal, using the phenomenon of electric discharges occurring between two electrodes in the presence of a dielectric, allows obtaining geometrically complex shapes that are difficult to obtain by other methods. EDM machining is divided into two major types: die-sink EDM and the wire-cut EDM. The following Fig. 2 shows the two machine types. The principals are the same for the Die-Sink as well as for Wire EDM process with a small difference in the setup. As it has been mentioned above, EDM is a removable process for conductive materials by means of rapid repetitive spark discharges in the presence of dielectric liquid, while a voltage difference is applied between the electrode and workpiece.

Physical phenomena that occur during the material removal process in an erosion process are of a complex nature. As a result of the applied electrical voltage, in the presence of dielectric fluid (usually deionized water or hydrocarbon oil, which acts as an insulator and coolant) the electrode comes closer to the workpiece material. Upon the conductive workpiece, a column of intense electromagnetic flux is formed. The electrical field is the strongest (energy density of 1011–1014 W/m$^2$) at the point where the distance between the electrode and workpiece is minimum. As the insulating effect of the dielectric fluid breaks down under high electric field, it causes a single spark to be discharged between the tool electrode and the workpiece. EDM utilizes the material erosion due to a spark, occurring between two electrodes, one of which is the workpiece, while both are immersed in the dielectric fluid. The intense electromagnetic flow forms a plasma channel, with plasma temperatures being in the range of 8000–12,000 °C. Part of the discharge energy is transformed into thermal energy, and a part of it is absorbed by the workpiece; as a result, an amount of material is melted and/or ablated. A portion of the molten and ablated material is being flushed away by the dielectric fluid, after the end of the current pulse, and the consequent breakdown of the plasma channel. A series of thousands or even millions of pulses and sparks per second result to the total material removal. This cycle is repeated many times during the machining process. The typical Material Removable Rate (MRR)
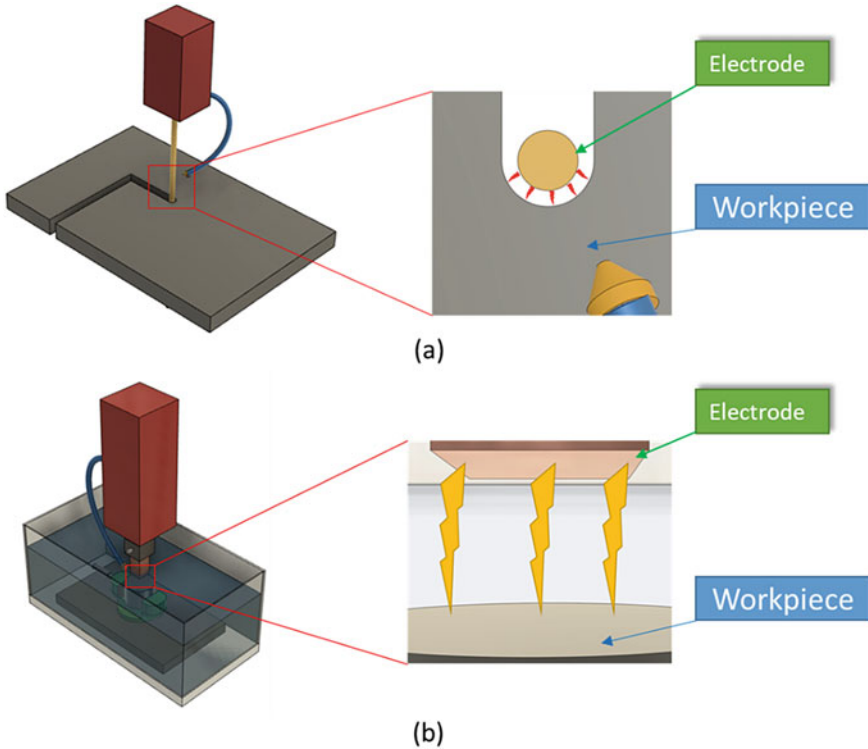
**Fig. 2** Graphical representation of **a** Wire EDM and **b** Die-sink EDM

per discharge is in range of 10–6 to 10–4 mm$^3$, depending on the intensity of the specific application [7, 8]. Since the shaped electrode defines the area in which the spark erosion will occur, the accuracy of the part produced after EDM is fairly high.

In the case of Wire EDM (WEDM), uses a moving wire as a machining tool, whose diameter is between 0.02–0.5 mm to remove material. The workpiece geometry is obtained as a result of electrical dissipation between the wire electrode and the workpiece surface. The wire electrode moves along the programmed path, which allows cutting geometrically complex shapes. Depending on the required dimensions and dimensional accuracy and surface roughness of the cut elements, the treatment is carried out in several electrode passes along the programmed contour for cutting [9].

On the other hand, Die-Sink EDM the erosion mechanism occurs between the shape of the electrode and the workpiece; the geometry of the electrode is reproduced in the object with high accuracy. Modern electro-erosion machine tools are equipped with a numerical control system that enables the production of geometrically complex cavities or holes [10]. As a dielectric medium in die-sink EDM is used commonly hydrocarbon fluids, synthetic fluids or even vegetable oil-based fluids. The surface finish, as well as other parameters, relies on the dielectric decision of dielectric fluid [11].

# 3 Phases of Electrical Discharge

After 70 years of important applications of EDM in manufacturing processes, it is very difficult to present a complete and define model explaining in all the different processes that take place during one discharge. Makund et al. [12], presented the expanding-circle heat-source model that provides correct erosion curves and explains the low erosion rates. Almost one-decade, later Schumacher [13] tries to cover the gap between different authors and to create a new consensus base. The following Fig. 3 presents the faces of a single discharge pulse, namely:

1. The ignition phase.
2. Formation of the plasma channel.
3. Melting and evaporation of a small part of the workpiece material and the electrode.
4. Ejection of the liquid molten material.

**The ignition phase**

In the first stage of the process (Fig. 3a), there is a lack of current flux due to the resistance of the dielectric fluid. As the electrode comes closer to the workpiece material, the electric field is increased and occurs the primary emission of the cathode's
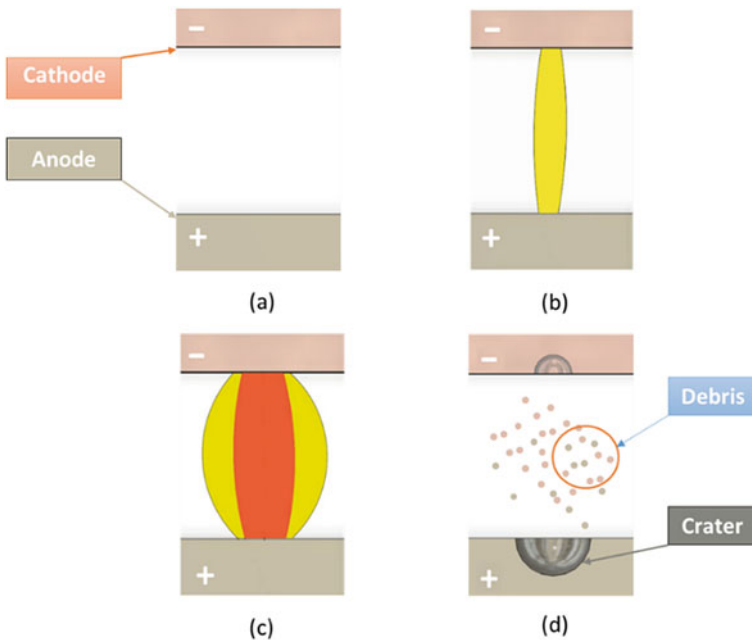


**Fig. 3** Graphical presentation of the discharge phases: **a** ignition, **b** plasma formation, **c** plasma channel expand, **d** flashing

electrons. These electrons accelerate by the electric field in the directions of the anode and hit the molecules of the dielectric. Thus, generates secondary electrons and positive ions that move, respectively, to the anode and the cathode causing the ionization.

**Formation of the plasma channel**

During this phase, the positive ions created from the dielectric collide with the electrodes from the cathode. This process produces more electrons that they are attached to the anode and liberates more electrons. This genesis superheating followed by small evaporation of the dielectric. This causes a reduction of the resistance of the dielectric and increasing the electrical current, creating a discharge tunnel. The plasma channel is created and circled by a vapor bubble, which concentrates all the energy in that small volume. At this moment the open-circuit voltage drops rapidly to the break voltage of the dielectric.

**Melting and vaporization of the electrode materials**

At this stage, during the generated plasma channel, the increased plasma high energy melts both electrodes by thermal conduction and a portion of the electrode evaporates due to the high plasma pressure over the cathode and anode spots. The explanation of this phenomenon could be that both anode and cathode surfaces are affected by the emission of the electrons and positive ions. The kinetic energy is transformed into thermal energy as in both cases, the positive ions or the electrons hit the cathode or the anode, respectively. As it can be in Fig. 3d, the anode melts quicker than the cathode, due to lower mass of the electrons that collide with the anode compared to the positive ions.

**Flushing of the melted material**

During the pause period, when the EDM machine stops the current abruptly, the plasma channel collapses and the vapor bubble is formed, causing the superheated molten liquid material of the surfaces (electrode and workpiece) to explode into the dielectric. A part of the material flashes out by the dielectric into the surrounding, while another part resolidifies in the crater. The last part of the material is called "White Layer" (WL) or recast layer. In Fig. 4, the crater formation during a single spark on tool steel utilizing a copper electrode with straight polarity is depicted. A part of the evaporated material has been flushed away, while another part formed a recast layer.

# 4  Process Parameters—Performance Indexes

Due to the multiparametric nature of the EDM, the process parameters can be branched into two categories, i.e. non-electrical and electrical parameters. The most important electrical parameters that affect the discharge energy are the Pulse-On time ($T_{on}$), the Pulse-on current ($I_p$), the duty factor and the polarity. On the other
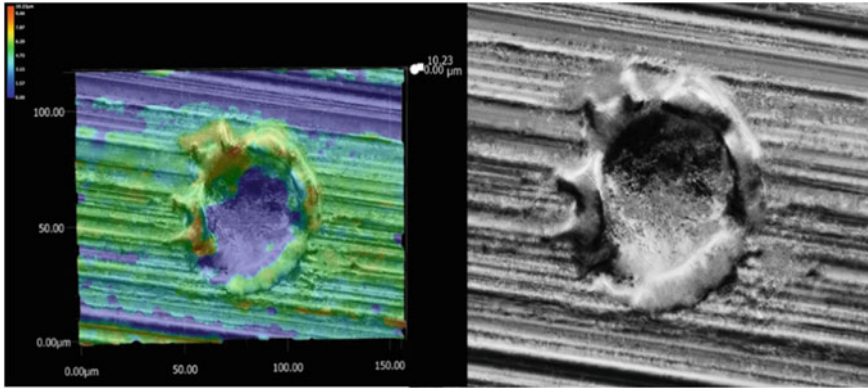
**Fig. 4** Crater formation from a single spark experiment

hand, these parameters are strongly related to the process parameters criteria (non-electrical) such as the Material Removable Rate (MRR), Tool Wear Ration, and the Surface Roughness (SR) [14, 15].

**The duration of a pulse ($T_{on}$)**

Is defined as the time during which there is a current flow between the electrode and the piece and consequently, the time period during which material expulsion is observed. The rate of material expulsion (MRR) is directly related with the machining parameters, especially with the pulse-on current and time, and the machining efficiency. Longer pulses result in a lower quality machined surface, as the craters formed are deeper and broader in diameter. For low roughness, the use of "shorter" pulses is recommended. Finally, the pulse duration of the pulses is related, to the processing speed and surface roughness, to the stability of the treatment.

**The pulse interval ($T_{off}$)**

The time between the occurrence of two pulses is defined as Pulse-off time. During it, there is no current flow, no spark event. Nevertheless, it is essential, as it is the time during which the waste—products—are removed from the treatment zone. Choosing the right interval is an optimization between the stability and the speed of the processing (increasing the interval makes the processing slower, but at the same time helps to remove the waste, making it more stable more effectively). Typical prices are of the class of μs.

**The Potential difference**

The potential difference between the piece and the electrode during processing is an essential parameter. Higher values allow for a more significant gap between the electrode and the piece, which makes it easier to flush and remove waste, making processing more stable and increasing the MRR. At the same time, however, it results in treated surfaces with higher surface roughness and more significant electrode wear.

**Material Removable Rate (MRR)**

It is defined as the volume of material that is removed at a specified reference time. It is usually expressed in units [mm$^3$/min] and is calculated indirectly by the weight difference of the piece before and after processing. It is an indicator of the processing speed and is affected by the current intensity, the pulse and interval time, the "duty cycle", and the properties of the material to be processed.

**Tool Wear Rate (TWR)**

In the literature, the tool wear ratio (TWR) is also found as an electrode wear ratio (EWR) or Relative Electrode Wear (REW). There is no difference, and it is essentially the ratio of the volume of material removed from the electrode to the volume of material removed from the piece expressed as a percentage [%]. There are cases where the wear of the electrode on the "front surface" or in the corners, you measure independently in [mm] or [μm]. Nevertheless, the electrode wear ratio (TWR) continues to be the most accurate method of measuring—expressing the wear of the electrode during processing. Understandably, the wear of the electrode must be clearly lower than that of the piece. Low TWR values express more stable, more efficient and more economical treatments. The wear ratio depends directly on the processing conditions (current intensity, vacuum potential, pulse time), the properties of the materials (electrode and piece), but also the polarity used [16].

**EDM in Steel Alloys**

Steel and its alloys, was one of the first materials that were used experimentally in EDM due to their use, mainly in production dies and molds. Until 1990, the workpiece surface quality was exanimated only by stylus profilometers without considering any material transformation and damage in ultramicroscopic level [17]. As the microscopic technology developed, researchers were able to obtain three-dimensional images of the surface topography as well as to define the particle migration, micro and macrocracks. Haron, Deros and Fauziach [18] investigated the influence of the EDM parameters on an AISI 1045 tool steel. The experimental results show that the MRR and TWR were not depended on the size of the electrode, but it was near related to the current flow. An experimental investigation was conducted by Bleys et al. [19], on the surface and sub-surface properties of tool steel machined by EDM. They considered three types of EDM processes, namely die-sink EDM, WEDM and Milling EDM (MEDM) and they found that the developed of new generators or mixed powder dielectrics will reduce the surface damage. Soni and Chakraverti [20, 21], investigated the TWR, MRR, surface texture, and the dimensional accuracy of steel alloys machined by EDM.

Several researchers [22–30] tried to improve EDM performance in order to increase machining production and decrease the machining time. The main aim is to increase the accuracy and the MRR but at the same time minimizing the TWR. As it has been abovementioned, due to the multiparametric nature of the EDM process, it is not easy to find a single optimal combination for the machining parameters. Thus,

there is a need to apply multi-objective optimization methods to find the solutions to these machining problems.

Khan [31] performed a comprehensive study by EDM mild steel by using copper and brass electrodes. The results show that TWR increases with the increase of voltage and current, also the cross-section of the electrode undergo more wear compared to its length. Guu et al. [32] investigated the surface characteristics of AISI D2 tool steel machined by EDM. They evaluated the recast layer by using Scanning Electron Microscopy (SEM) and X-ray diffraction technique and showed that, an excellent machine surface is produced with lower discharge energy, also at these conditions (lower pule-on time and current) reduces the tensile residual stress. Straka et al. [33] suggested an applied mathematical model to minimize the depth of Heat Affected Zone (HAZ) and the microhardness of an EN X32CrMoV12-28 steel machined by EDM with SF-Cu electrode. According to their study, the most significant parameters that affect the quality of the machined surface are the pulse-on and pulse-off time as well as the pulse-on current. A comparison study performed on a duplex stainless steel alloy machined by EDM with 3 different electrodes (Graphite, Copper-Tungsten and Tungsten electrodes) and 2 different dielectric mediums. Ablyaz et al. [34] found by using Taguchi L18 method that, the most significant parameter that affect the surface roughness is firstly the material of the electrode although for the MRR the dominated factor was the pulse-on current. The study also reported that higher MRR and SR values exhibited the surface wettability. Finally, Mouralova et al. [35] performed a comprehensive study on the influence of the WEDM parameters on Hardox 400 Steel. Among the other parameters ($I_p$, $T_{on}$, $T_{off}$ and V), they also analyzed the wire feed and the cutting feed. By using a regression model, the results show that the cutting speed is mainly affected by the pulse-on time and pulse-on current, while the recast layer was between 5 to 20 $\mu$m.

## EDM in Aluminum Alloys

Aluminum is light, ductile, plastic, non-magnetic; is an excellent conductor of electric current; quickly oxidizes; it is very resistant to tarnishing; is recycled. Aluminum is the third most abundant element (and the most abundant metal) in the earth's crust, which is about 8.1% by mass. It is a reactive element that forms solid compounds, so a lot of energy is required to obtain aluminum from aluminum oxide. As the injection mold technology was getting more and more popular during the past two decades, aluminum molds are competing with harden steel to produce softer materials. Thus, a lot of researchers tried to explore the advantages of machining aluminum and its alloys by using EDM technology [7]. Rao, Ramji and Satyanarayana [36, 37] investigated the generated conditions of residual stresses in Machining AA2014 T6 by using WEDM. The results reviled, a wide range of residual stresses from 8.2 MPa to 405.6 MPa. Besides, the researchers noticed the presence of AlCu and $ACu_3$ intermetallic. These stresses could cause a susceptible surface to crack formation, which affects not only the corrosion and wear resistance [38, 39] but also the fatigue life [40]. Khana et al. [41] performed an EDM drilling on aluminum alloy 7075. By using Taguchi grey relational theory and ANOVA they were able to analyze the response factors (MRR and TWR) and correlate them with the machining parameters

in order to find the optimal drilling conditions. They also Reported that the MRR and TWR are mainly affected of the pulse-on and off time. By using the same statistical method Bobbili and Gogia [42] machined a ballistic grade aluminum alloy by WEDM. Mathematical models were developed using response surface method to determinate the correlation between machining and performance characteristics. It was demonstrated by Ahmed [43] an experimental investigation of coating deposition on aluminum by EDM. The results show that most significant parameter that affect the layer thickness, material deposition rate and the TWR is the peak current ($I_p$). In addition, the surface microhardness had a significant improvement with an average hardness of 640HV.

## 5   Modeling and Simulation of EDM

Modeling and simulation consist a powerful tool in research regarding the EDM process. Additionally, except of the capability to predict the machining results, it provides an insight of the process, allowing the study of mechanisms and phenomena that are almost impossible to be experimentally studied. Since EDM is a multi-parameter process, with complex physical phenomena to take place, some reasonable simplifications and assumptions have to be made, in order the modeling to become feasible. These assumptions have always to be scientifically justified, and be based on robust theoretical background. Each researcher/research team, adopts its own approach regarding the simulation of EDM, developing and presenting different models. Nevertheless, some assumptions/simplifications are common, thus, it is considered useful and helpful to be presented.

At first, all discharges are considered identical, while during each pulse only one spark is occurred. Thus, this "average" spark is simulated, and the results concerning the overall process deduced from correspondence to the real processing time. The into material heat transfer is considered that mainly take place due to conduction, while Joule heating is often neglected. [44] The plasma channel is the main heat source, while the workpiece exchanges heat through convection with the dielectric fluid, and through radiation. Finally, the workpiece material is assumed as isotropic. Some more details will be discussed below.

The conduction heat transfer is mathematically described as:

$$\rho \cdot C \cdot \frac{\partial T}{\partial t} - \nabla \cdot (k \cdot \nabla T) = Q \tag{1}$$

with T the temperature, $\rho$ the density, C the heat capacity (at a constant pressure $C_P$, or for a constant volume $C_v$), k the thermal conductivity and Q a heat source or a heat sink. The heat source, i.e. the plasma channel in most simulations is considered to have a Gaussian distribution, hence, the power density can mathematically be expressed:

$$Q(r) = 4.57 \cdot \frac{F_W \cdot V \cdot I_P}{\pi \cdot R_P^2} \cdot e^{-4.5 \cdot \frac{r^2}{R^2}} \tag{2}$$

with V the machining voltage in V, $I_p$ the pulse-on current in A, $R_p$ the plasma channel radius in m, r the distance from the center of the plasma channel in m, and $F_w$ the proportion of energy that is absorbed by the workpiece. At this point, some important clarifications have to be made. At first, and regarding the power distribution of the heat source: in studies different types of heat sources have been adopted, namely, point heat source, or disc heat source. Nevertheless, in many of the models, a heat sources with a Gaussian distribution is utilized, not only because the obtained results are in line with experimental ones, but due to the theoretical background that supports this approach. In the work of Weingärtner et al. [45] a comprehensive comparison between different heat sources models can be found, concluding that the Gaussian distribution is the most consistent with experimental results. Moreover, and regarding the plasma channel radius, there is not a generally accepted model for its calculation, rather experimentally driven semi-empirical relations. Two commonly used relations are [46]:

$$R_p = 2.04 \cdot I_P^{0.43} \cdot T_{on}^{0.44} \tag{3}$$

with $R_P$ the plasma channel radius in $\mu$m, $I_p$ the discharge peak current in A and $T_{on}$ the discharge duration in $\mu$s.

$$R_p = 0.85 \cdot 10^{-3} \cdot I_P^{0.48} \cdot T_{on}^{0.35} \tag{4}$$

with $R_p$ the plasma channel radius in m, $I_p$ the discharge peak current in A and $T_{on}$ the discharge duration in s. Additionally, in some simulations the plasma channel is considered constant during the whole spark time [47], while in others, the plasma channel growths over time [48], implementing an expanding heat source. Finally, in order the heat source to be fully described, the proportion of power that is absorbed by the workpiece must be defined. Again, there is a deviation between the adopted coefficients. In lots of studies an absorption coefficient of 18.3% is utilized, which emanates from the research of DiBitonto et al. [12]. But this is only an approach; for example, Vishwakarma et al. [49] used an absorption coefficient of 8%, while Singh defined an absorption coefficient between 6.1 and 26.82%. The proportion of energy that is absorbed by the workpiece is strongly depends on the machining parameters, the workpiece and the electrode material, hence, these coefficients must carefully be adopted and as the case may be. The most proper approach, in order the accuracy to be ensured, is its definition by reverse engineering, based on experimental results. Furthermore, this coefficient is preferably not to be constant, but as function of the machining parameters [50].

The convection heat transfer between the workpiece and the dielectric fluid is expressed as:

$$q_{diel} = h_{diel} \cdot (T - T_{diel}) \qquad\qquad (5)$$

with $q_{diel}$ the heat flux from the workpiece to dielectric fluid due to convection in $W/m^2$, $h_{diel}$ the heat transfer coefficient between the workpiece and the dielectric oil in $W/m^2K$.

At this point, it should be pointed out that in most of the models the assumption of a constant geometry is implemented. In other words, the material erosion is not considered, and the material removal is estimated through a temperature condition. In a different approach, the material erosion is taken into consideration and simulated, through computational methods like moving mesh [51] or deformed geometry [52]. Finally, it must mention, that there are studies concerning consecutive spark, and the surface morphology as the result of them [53]. In those models, a multi-scale approach is adopted, coupling the single spark analysis with a macro scale analysis, where conclusions regarding the surface characteristics and roughness can be deduced.

## 6   Case Study: The Machining of Aluminum Alloys Al5052 and Al6063 with EDM

The current case study concerns the machining of two different aluminum alloys with EDM, namely the Al5052 and Al6063. The same machining parameters were utilized, aiming in a straight comparison of the machining results, regarding the MRR, Ra and Rt. Al5052 nominally contains 2.5% magnesium & 0.25% chromium, has good workability, very good corrosion resistance, high fatigue strength, weldability, and moderate strength, while it is extensively used in aircraft fuel/oil lines, fuel tanks and other transportation areas. In Al6063 the basic alloying elements are the magnesium (0.45–0.9%) and the silicon (0.20–0.6%), it is a medium strength alloy, with a wide range of applications, including architectural and transportation applications. The alloys' detailed chemical compositions along with their mechanical and thermophysical properties are listed in Table 1.

The experiments were carried out on an ANGIETRON EMT 1.10 die sinking EDM machine, by using aluminum plates as workpiece material, and utilizing copper working electrode, with nominal dimensions of 38 × 23 mm. In order any depositions accumulation on electrode's surface to be avoided, in-between the experiments the electrode was properly being cleaned. A highly purified synthetic hydrocarbon oil was used as dielectric fluid, which was properly channeled into the working tank for the efficient debris removal. A nominal 1 mm cutting depth was set for all the experiments, in order a full and uniform machined surface to be formed.

A full-scale experiment was conducted, with control parameters the pulse-on current and time, each of one taking 4 levels of values, thus, 32 experiments were carried out in total. The pulse-on current and time varied from 15 up to 24A and from 100 up to 500 μs respectively, covering that way a wide range of per pulse energies. In Table 2, the machining parameters are listed in details. The experiments

**Table 1** Chemical composition, mechanical and thermophysical properties of Al5052 and Al6063

Chemical composition

| Element Wt. % | Al | Cr | Cu | Fe | Mg |
|---|---|---|---|---|---|
| Al5052 | 95.7–97.7 | 0.15–0.35 | ≤0.1 | ≤0.4 | 2.2–2.8 |
| Al6063 | ≤97.5 | ≤0.1 | ≤0.1 | ≤0.35 | 0.45–0.9 |
| Element Wt. % | Mn | Si | Ti | Zn | Other total |
| Al5052 | ≤0.1 | ≤0.25 | – | ≤0.1 | ≤0.15 |
| Al6063 | ≤0.1 | 0.2–0.6 | ≤0.1 | ≤0.1 | ≤0.15 |

Mechanical and thermophysical properties

| | Density [g/cc] | Cp [J/kgK] | Thermal cond. [W/mK] | Melting point [K] | Electrical resistivity [ohm/cm] | HV |
|---|---|---|---|---|---|---|
| Al5052 | 2.68 | 880 | 138 | 880–922 | 499e-8 | 68 |
| Al6063 | 2.70 | 900 | 200 | 889–927 | 332e-8 | 83 |

**Table 2** Machining parameters

| Machining conditions | Level 1 | Level 2 | Level 3 | Level 4 |
|---|---|---|---|---|
| Discharge current $I_p$ (A) | 15 | 18 | 21 | 24 |
| Pulse on-Time $T_{on}$ (μs) | 100 | 200 | 300 | 500 |
| Dielectric | Synthetic hydrocarbon fluid | | | |
| Dielectric flushing | Side flushing | | | |
| Open circuit voltage (V) | 100 | | | |
| Close circuit voltage (V) | 30 | | | |

were conducted under straight polarity, with constant voltage difference, and more specific, 100 and 30 V nominal open and close circuit voltage respectively. The Duty Factor (η) was automatically adjusted to optimize the process, thus, only indirectly can be estimated based on the mean current. Taking in mind that voltage pulses can be approximated by square pulses, the Duty Factor is calculated based on Eq. 6:

$$\eta = \frac{\overline{I_p}}{I_p} \tag{6}$$

with Īp with the ammeter indication of the mean current intensity in A and $I_p$ the nominal pulse-on current in A. The MRR is defined as the volume of the removed material per minute, and calculated based on Eq. 2:

$$MRR = \frac{W_{st} - W_{fin}}{\rho \cdot t_m} \tag{7}$$

with MRR the material removal ratio in gr/min, $W_{st.}$, $W_{fin}$ the workpiece weight before and after machining, respectively, in gr, ρ the workpiece material density in gr/mm$^3$ and tm the machining time in min.

The Surface Roughness was estimated in terms of Ra and Rt, which emerged as the mean value of five consecutive measurements on each machined surface. Finally, the machined surfaces cross sections were grinded, polished and chemically treated with proper etchant, being composed of 92 ml distilled water, 6 ml nitric acid and 2 ml hydrofluoric acid and the etched surfaces were observed in optical microscope in order the formed WL to be studied.

## Experimental Results and Discussion

In Table 3 the experimental results are presented.

MMR consists one of the main productivity indexes, directly related with the machining efficiency and sustainability. Although, it is strongly depending on the machining parameters, namely the pulse-on current and the pulse-on time, there is not a linear correlation between the MRR and the machining power and the per pulse energy. More specific, an increase in the machining power, or in the per-pulse energy, does not compulsively result an increase in MRR, as there is an upper limit on the attainable MRR. This behavior can be attributed to three main reasons: the plasma channel growth, the debris concentration in between the electrode and the

**Table 3** Experimental Results

| $I_p$ [A] | $T_{on}$ [µs] | Al5052 | | | Al6063 | | |
|---|---|---|---|---|---|---|---|
| | | MRR [mm$^3$/min] | Ra [µm] | Rt [µm] | MRR [mm$^3$/min] | Ra [µm] | Rt [µm] |
| 15 | 100 | 172.7 | 10.8 | 77.2 | 125.66 | 8.10 | 53.40 |
| 18 | 100 | 207.3 | 10.7 | 76.6 | 189.49 | 9.30 | 62.40 |
| 21 | 100 | 207.3 | 11.2 | 76.2 | 148.15 | 9.10 | 64.80 |
| 24 | 100 | 257.3 | 11.8 | 86.4 | 211.64 | 10.30 | 77.60 |
| 15 | 200 | 179.7 | 15.1 | 95.6 | 139.65 | 11.20 | 67.80 |
| 18 | 200 | 213.2 | 14.5 | 98 | 189.30 | 12.40 | 88.60 |
| 21 | 200 | 252.1 | 14.4 | 96.8 | 194.00 | 11.80 | 83.40 |
| 24 | 200 | 274.4 | 14.5 | 101.6 | 233.92 | 13.40 | 85.80 |
| 15 | 300 | 155.5 | 14.1 | 93.8 | 129.63 | 14.20 | 89.20 |
| 18 | 300 | 216.9 | 16 | 113.2 | 161.62 | 14.20 | 96.40 |
| 21 | 300 | 223.9 | 15.2 | 104.2 | 189.30 | 13.80 | 101.00 |
| 24 | 300 | 259.1 | 14.4 | 104.4 | 219.91 | 15.00 | 94.00 |
| 15 | 500 | 176.7 | 14.2 | 94.4 | 133.10 | 13.70 | 94.80 |
| 18 | 500 | 223.9 | 17.1 | 114.8 | 177.13 | 16.00 | 101.40 |
| 21 | 500 | 234.3 | 16.7 | 105 | 170.37 | 13.60 | 85.80 |
| 24 | 500 | 279.9 | 19.4 | 140.6 | 202.82 | 16.70 | 110.20 |

workpiece and the deposition of carbon the electrode surface. The formed plasma channel expands over the pulse time, consuming significant amounts of energy. Hence the higher the pulse-on time is, the more power is consumed by the plasma channel, decreasing the machining efficiency. At the same time, intense machining parameters lead in increased debris concentration between the electrode and the workpiece, acting like a physical barrier, while a significant amount of energy is spent as they re-melt. The carbon that is decomposed due to high temperatures is being deposited on the surface of the electrode and workpiece, forming a "shield layer" of carbides, which decrease the process efficiency. These underlying mechanisms that taking place during machining significantly affect the MRR, hence, it is of extreme interest to be studied the response of MRR in respect of pulse-on current and time.

Based on the obtained experimental data, which are presented in Table 3, the comparison of MRR for the two aluminum alloys are presented in Fig. 5, along with the corresponding Main Effects Plots. At first, by analyzing the Main Effects Plot of both alloys, it can be deduced that the pulse-on current is the major parameter that mainly affects the MRR, while the pulse-on time has a slight and vaguer influence. More specific, for the Al5052, the mean MRR is constantly increased with increase of $I_p$, having a total 56.4% increase as pulse-on current is increased from 15 to 24A. On the other hand, as the pulse-on time increased from 100 to 500 $\mu$s, the mean MRR only slightly changed, with the pulses of 100–300 $\mu$s, and 200–500 $\mu$s having almost the same mean MRR. Similar results emerged for the Al6063 as well. The pulse-on
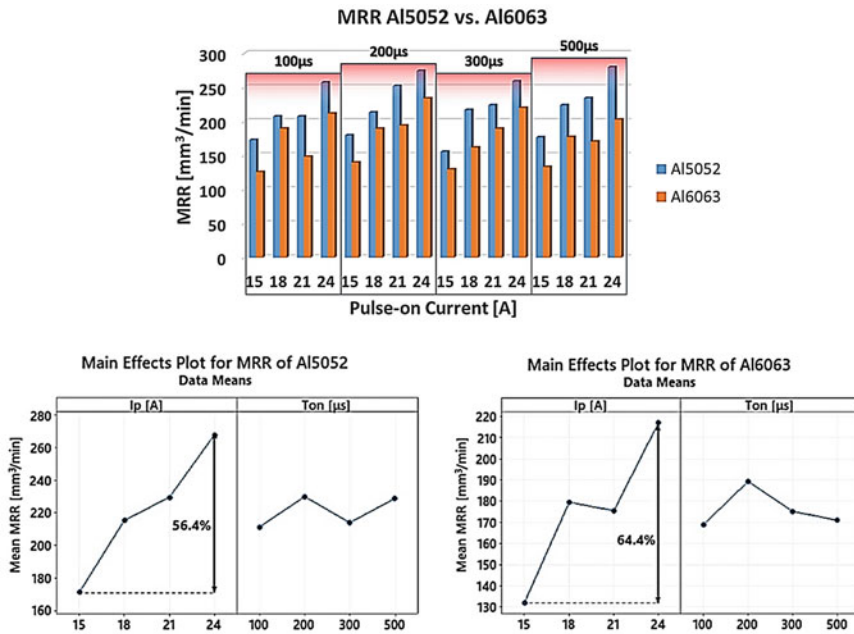


**Fig. 5** MRR for Al5052 and Al6063 along with the Main Effects Plot

current mainly affects the MRR, while the pulse-on time has a fuzzy influence. The mean MRR was increased about 64.4% as the $I_p$ increased from 15 to 24A, having only a small decrease between 18 and 21A. On the contrary, as the $T_{on}$ increased from 100 to 300 and 500 $\mu$s the mean MRR remained almost constant, with only a slight increase for pulse-on time 200 $\mu$s.

Comparing the MRR values of Al5052 and Al6063, for all the sets of machining parameters the MRR of Al5052 is higher, by average 26.36%. This can be attributed to the alloys' thermophysical properties. Namely, Al6063 has higher Specific Heat, Thermal Conductivity and Melting Point than Al5052. Hence, the absorbed energy is more easily distributed in the material, preventing the topical temperature rise that will lead in material melt and removal. At the same time, due to the higher Specific Heat and Melting Point, Al6063 requires more heat energy than Al5052 to be melt, leading in lower MRRs, compared with these of Al5052.

The machined Surface Roughness is another important parameter of EDM, straight related with the surface quality of components that been manufactured with EDM. The Surface Roughness highly depends on the pulse-on current and time, i.e. the machining power and the per-pulse energy. The roughness is the result of the material removal and the craters formation, as well the growth of the White Layer. The craters' geometrical characteristics, (e.g. size, depth and width) are contingent on the pulse-on current and time. Nevertheless, each parameter affects the craters' formation in a distinctive way. Specifically, and as a rule of thumb, the pulse-on time allows the plasma channel to expand, resulting relatively big craters, while the pulse-on current mainly is reflected on the depth of the formatted craters. Nevertheless, the SR is subject to complicated underlying mechanisms, and depends on numerous of parameters, including the workpiece and electrode material, the dielectric fluid, the applied voltage and the utilized polarity during machining. Additionally, a crucial parameter in Surface Quality, and hence for SR is the formation of the WL. During EDM, only a portion of the molten material is removed from the workpiece, with the rest of it being re-solidified. Moreover, ablated material, and debris that remained in a close proximity to the workpiece surface, may re-attaches themselves, as a layer, on the spark cavity forming a layer of re-deposited material. The re-solidified and the re-deposited material form the WL, that drastically reshape the Surface Topology, since the morphology of the machined surface is not only developed by consecutive and/or overlaying craters, but from complex formations of re-solidified and re-condensed material. In Figs. 6 and 7 Ra and Rt of the machined surfaces are presented, along with their Main Effects Plots.

On the contrary with MRR, the Ra is mainly affected by the pulse-on time, while the pulse-on current has a minor, and vaguer influence. More specific, the mean Ra of Al5052 is constantly increased with increase in pulse-on time, having 51.5% higher mean value for $T_{on}$ 500 $\mu$s, compared with the mean value for 100 $\mu$s pulse-on time. On the other hand, the mean Ra for the different pulse-on currents does not significantly change, showing only a slight increase trend as the pulse-on time (i.e. the machining power) increases. Similarly, in Al6063, increase in pulse-on time results a continuous increase in mean Ra, while, the utilization of higher pulse-on current has a fuzzy affect, leading in both increase and decrease of the mean Ra.
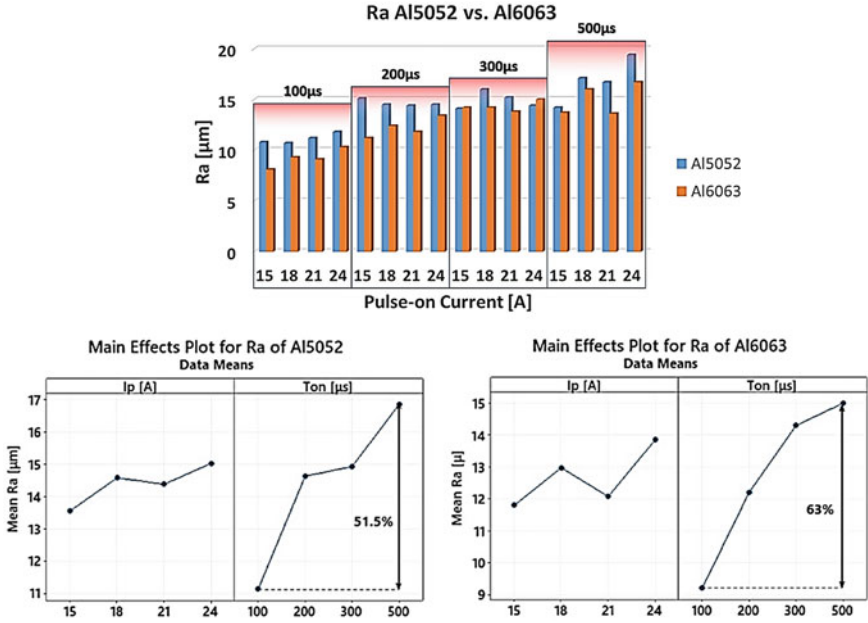
Ra Al5052 vs. Al6063

Fig. 6 Ra for Al5052 and Al6063 along with the Main Effects Plot
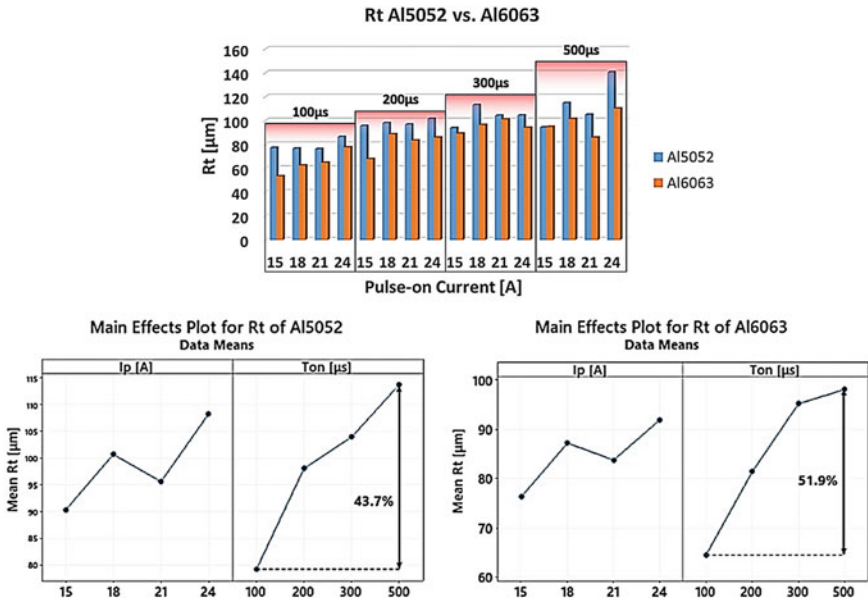
Rt Al5052 vs. Al6063

Fig. 7 Rt for Al5052 and Al6063 along with the Main Effects Plot

Comparing the values of Ra for both alloys, they are in the same order of magnitude, with the Ra of Al5052 being, in the vast majority, higher. This can be reasonably attributed to the lower Thermal Conductivity, Specific Heat and Melting Point of Al5052, parameters that, as it has been aforementioned, affect the MRR. Namely, the higher MRR of Al5052, implies that on each spark a greater amount of material is removed, forming a bigger crater.

As it was expected, Rt is mainly affected by the pulse-on time, while the pulse-on current has a fuzzy influence. As the $T_{on}$ increases, the mean Rt also continuously increases, for both alloys, having a 43.7% and 51.9% rise between 100 and 500 μs for the Al5052 and Al6063 respectively. On the other hand, higher pulse-on currents result either an increase or decrease of the mean Rt, hence, any conclusion could be precarious. Finally, it has to be mentioned, that, with only one exception, the Rt of Al5052 is higher than this of Al6063, advocating that in machining of Al5052 bigger and deeper craters are formed.

In Figs. 8 and 9 the cross sections of Al5052 and Al6063 are depicted respectively, for constant machining power (i.e. 24A pulse-on current), and for different per pulse energies (i.e. 100, 200, 300 and 500 μs). Observing the cross sections, it is deduced that the morphological characteristics of the WL are strong related with the pulse-on time. Namely, for $T_{on}$ 100 μs, in both alloys, the WL is thin discontinuous, more like random formations on the surface. Moreover, the formatted craters that can be distinguished are shallow and wide. For 200 μs pulse-on time, the WL becomes thicker, covering greater percentage of the surface. Furthermore, some hollow globules appear, while the formed craters become deeper. The hollow formations are shaped as the result of the material's rapid re-solidification, and the gas entrapment
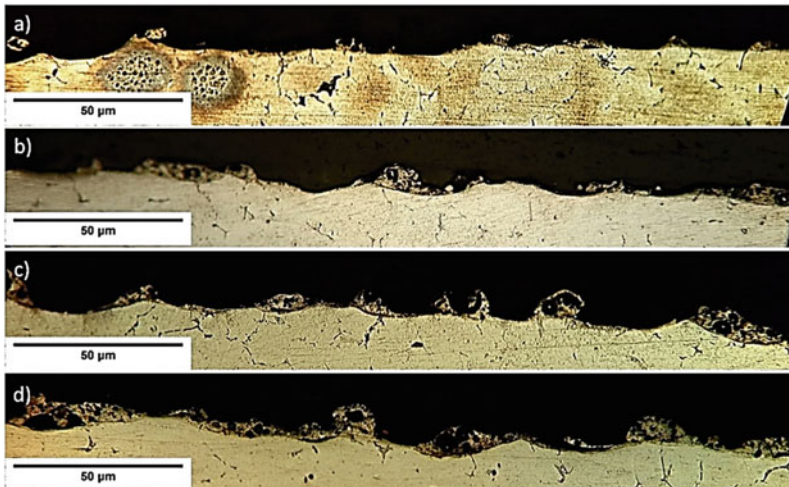


**Fig. 8** Surface cross sections of Al5052 for 24A and pulse-on time **a** 100 μs, **b** 200 μs, **c** 300 μs, **d** 500 μs
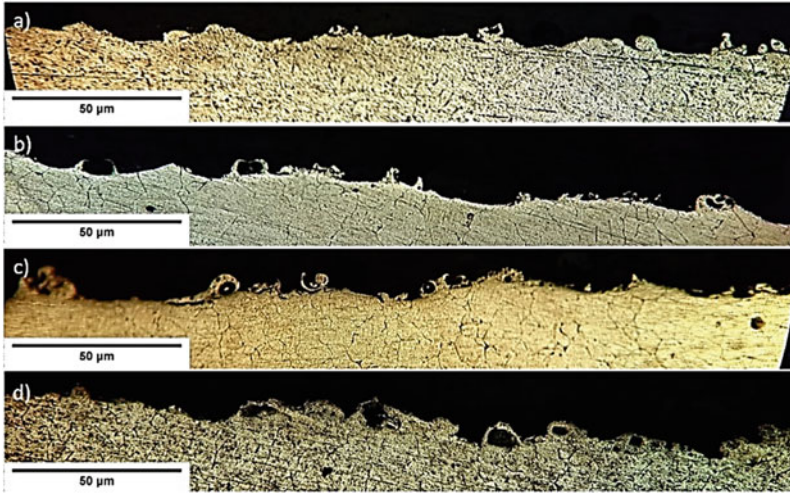
**Fig. 9** Surface cross sections of Al6063 for 24A and pulse-on time **a** 100 μs, **b**) 200 μs, **c** 300 μs, **d** 500 μs

inside it. For higher pulse-on times (300 and 500 μs), the WL get almost continuous and thicker, while the aforementioned globules become denser and more bulky.

The juxtaposition of the cross sections for different per pulse energies, and for both alloys, confirm the results of Ra and Rt, which previously presented and analyzed. The WL in Al5052 is thicker in comparison with that of Al6063, while the formed craters appear to be deeper and the globules more bulky. For all those reasons, it is justified that Ra and Rt are higher in Al5052, and their increase in respect of the pulse-on time.

## 7 Summary

The current chapter concerns the non-conventional machining process of EDM, as well a specific case-study, namely, the machining of aluminum alloys Al5052 and Al6063 with EDM. After a brief historical review, the main operation principles and the underlying mechanisms of the process were presented, along with the most widely used performance indexes. Then a brief review was presented for the machining of steel and aluminum alloys with EDM, providing an adequate relevant literature. In Sect. 5, the basic principles of modeling and simulation of EDM were presented, while some interesting and "scientifically open" issues were pointed out. Finally, in the last section a case study regarding the comparison of machining Al5052 and Al6063 with EDM was presented. A full-scale experiment was carried out, with control parameters the pulse-on current and time. The machining performances were estimated in terms of Material Removal Rate and Surface Roughness (Ra, Rt), while

the machined surfaces cross sections were studied in optical microscope, in order the WL formation to be observed. It was deduced that the pulse-on current mainly affects the MRR, while Ra and Rt mainly depend and affected by the pulse-on time. Finally, it was concluded that the WL morphology is contingent on both the machining parameters, and the workpiece material as well.

# References

1. Ho KH, Newman ST (2003) State of the art electrical discharge machining (EDM). Int J Mach Tools Manuf 43:1287–1300. https://doi.org/10.1016/S0890-6955(03)00162-7
2. Markopoulos AP, Papazoglou E-L, Karmiris-Obratański P (2020) Experimental study on the influence of machining conditions on the quality of electrical discharge machined surfaces of aluminum alloy Al5052. Machines 8:12
3. Priestley J (1775) Experiments on the circular spots made on pieces of metal by large electrical explosions. The history and present state of electricity with original experiments, vol. II, 3rd ed. London
4. BR, Lazarenko NJ (1944) Electrical erosion of metals. In Russian: gosenergoisdat leningrad, 27 p, 7 figures
5. Webzell S (2001) That first step into EDM, Machinery, 159, (4040) Findlay Publications Ltd. UK, Kent, p 41
6. Ho KH, Newman ST, Rahimifard S, Allen RD (2004) State of the art wire electrical discharge machining. Int J Mach Tools Manuf 44:1247–1259
7. Markopoulos AP, Papazoglou EL, Svarnias P, Karmiris-Obratański P (2019) An experimental investigation of machining aluminum alloy Al5052 with EDM. Procedia Manufacturing 41:787–794
8. Descoeudres A (2006) Characterization of electrical discharge machining plasmas, PhD thesis, ÉCOLE POLYTECHNIQUE FÉDÉRALE DE LAUSANNE, THÈSE NO, 3542
9. Xu CS (2012) Working principle and performance of wire electrical discharge machining. Adv Mater Res 507:180183. https://doi.org/10.4028/www.scientific.net/amr.507.180
10. Maradia U, Boccadoro M, Stirnimann J, Beltrami I, Kuster F, Wegener K (2012) Die-sink EDM in Meso-Micro Machining, Procedia CIRP, Volume 1. ISSN 166–171:2212–8271. https://doi.org/10.1016/j.procir.2012.04.029
11. Yunus Khan Mohd, Sudhakar Rao P, Pabla BS (2020) Investigations on the feasibility of Jatropha curcas oil based biodiesel for sustainable dielectric fluid in EDM process. Mater Today: Proc 26, Part 2. ISSN 335–340:2214–7853. https://doi.org/10.1016/j.matpr.2019.11.325
12. Di Bitonto DD, Eubank PT, Patel MR, Barrufet MA (1989) Theoretical models of the electrical discharge machining process. I. A simple cathode erosion model. J Appl Phys 66:4095–4103
13. Schumacher BM (2004) After 60 years of EDM the discharge process remains still disputed. J Mater Process Technol 149:376–381
14. Nikalje AM, Kumar A, Srinadh KVS (2013) Influence of parameters and optimization of EDM performance measures on MDN 300 steel using Taguchi method. Int J Adv Manuf Technol 69:41–49. https://doi.org/10.1007/s00170-013-5008-8
15. Karmiris-Obratański P, Zagórski K, Papazoglou EL et al (2020) Surface texture and integrity of electrical discharged machined titanium alloy. Int J Adv Manuf Technol. https://doi.org/10.1007/s00170-020-06159-z
16. Ciubotariu V, Câcu A, Rotundu I, Cucos M-M, Coteata M (2014) Influence of some factors on surface roughness parameters at electrical discharge machining. Appl Mech Mater 657:291–295
17. Guu YH (2005) AFM surface imaging of AISI D2 tool steel machined by the EDM process. Appl Surf Sci 242(3–4):245–250. https://doi.org/10.1016/j.apsusc.2004.08.028

18. Che Haron CH, Deros BM, Ginting A, Fauziah M (2001) Investigation on the influence of machining parameters when machining tool steel using EDM. J Mater Process Technol 116(1):84–87. https://doi.org/10.1016/s0924-0136(01)00846-9
19. Bleys P, Kruth J-P, Lauwers B, Schacht B, Balasubramanian V, Froyen L, Van Humbeeck J (2006) Surface and sub-surface quality of steel after EDM. Adv Eng Mater 8:15–25. https://doi.org/10.1002/adem.200500211
20. Soni JS, Chakraverti G (1991) Investigative study on metal removal rate and wear ratio in EDM of high carbon high chromium die steel J. Ind, Eng., p 71
21. Soni JS, Chakraverti G (1995) Effect of electrode material properties on surface roughness and dimensional accuracy in electro-discharge machining of high carbon high chromium die steel. J Ind Eng 76:46–51
22. Zarepour H, Tehrani AF, Karimi D, Amini S (2007) Statistical analysis on electrode wear in EDM of tool steel DIN 1.2714 used in forging dies. J Mater Process Technol 187–188:711–714. https://doi.org/10.1016/j.jmatprotec.2006.11.202
23. Lin CL, Lin JL, Ko TC (2002) Optimisation of the EDM process based on the orthogonal array with fuzzy logic and gray relational analysis method. Int J Adv Manuf Technol 19:271–277. https://doi.org/10.1007/s001700200034
24. El-Taweel TA (2006) Parametric study and optimisation of wire electrical discharge machining of Al–Cu–TiC–Si P/M composite. Int J Mach Machinab Mater 1(4):380–395. https://doi.org/10.1504/IJMMM.2006.012348
25. Su JC, Kao JY, Tarng YS (2004) Optimisation of the electrical discharge machining process using a GA-based neural network. Int J Adv Manuf Technol 24:81–90
26. Kuriakose S, Shunmugam MS (2005) Multi-objective optimization of wire-electro discharge machining process by non-dominated sorting genetic algorithm. J Mater Process Technol 170:133–141. https://doi.org/10.1016/j.jmatprotec.2005.04.105
27. Tsai KM, Wang PJ (2001) Semi-empirical model of surface finish on electrical discharge machining. Int J Mach Tools Manuf 41:1455–1477. https://doi.org/10.1016/S0890-6955(01)00015-3
28. Wang PJ, Tsai KM (2001) Semi-empirical model on work removal and tool wear in electrical discharge machining. J Mater Process Technol 114:1–17. https://doi.org/10.1016/S0924-0136(01)00733-6
29. El-Taweel TA (2009) Multi-response optimization of EDM with Al–Cu–Si–TiC P/M composite electrode. Int J Adv Manuf Technol 44:100–113. https://doi.org/10.1007/s00170-008-1825-6
30. Straka Ľ, Hašová S (2018) Optimization of material removal rate and tool wear rate of Cu electrode in die-sinking EDM of tool steel. Int J Adv Manuf Technol 97:2647–2654. https://doi.org/10.1007/s00170-018-2150-3
31. Khan AA (2008) Electrode wear and material removal rate during EDM of aluminum and mild steel using copper and brass electrodes. Int J Adv Manuf Technol 39:482–487. https://doi.org/10.1007/s00170-007-1241-3
32. Guu YH, Hocheng H, Chou CY, Deng CS (2003) Effect of electrical discharge machining on surface characteristics and machining damage of AISI D2 tool steel. Mater Sci Eng A 358(1–2):37–43. https://doi.org/10.1016/s0921-5093(03)00272-7
33. Straka L, Corný I, Pitel' J, Hašová S (2017) Statistical approach to optimize the process parameters of HAZ of tool steel EN X32CrMoV12-28 after Die-Sinking EDM with SF-Cu Electrode. Metals 7:35
34. Ablyaz TR, Shlykov ES, Muratov KR, Mahajan A, Singh G, Devgan S, Sidhu SS (2020) Surface characterization and tribological performance analysis of electric discharge machined duplex stainless steel. Micromachines 11:926
35. Mouralova K, Benes L, Bednar J, Zahradnicek R, Prokes T, Fries J (2020) Analysis of machinability and crack occurrence of steels 1.2363 and 1.2343ESR Machined by Die-Sinking EDM. Coatings, 10, 406
36. Rao PS, Ramji K, Satyanarayana B (2014) Effect of wire EDM conditions on generation of residual stresses in machining of aluminum T6 alloy. Alexandria Eng J 55(2). ISSN 1077–1084:1110–168. https://doi.org/10.1016/j.aej.2016.03.014

37. Pujari SR, Koona R, Beela S (2018) Surface integrity of wire EDMed aluminum alloy: a comprehensive experimental investigation. J King Saud Univ—Eng Sci 30(4). ISSN 368–376:1018–3639. https://doi.org/10.1016/j.jksues.2016.12.001
38. Capello E (2004) Residual stresses in turning: Part I: influence of process parameters. J Mater Process Technol 160(2):221–228
39. Bonny K, De Baets P, Quintelier J, Vleugels J, Jiang D, Van der Biest O, Lauwers B, Liu W (2010) Surface finishing: impact on tribological characteristics of WC–Co hardmetals Tribology. Int 43:40–54
40. Ghanem F, Fredj NB, Sidhom H, Braham C (2011) Effects of finishing processes on the fatigue life improvements of electro-machined surfaces of tool steel Int. J Adv Manuf Technol 52:583–595
41. Khanna R, Kumar A, Garg MP et al (2015) Multiple performance characteristics optimization for Al 7075 on electric discharge drilling by Taguchi grey relational theory. J Ind Eng Int 11:459–472. https://doi.org/10.1007/s40092-015-0112-z
42. Ravindranadh Bobbili V, Madhu AKG (2015) Multi response optimization of wire-EDM process parameters of ballistic grade aluminium alloy. Eng Sci Technol Int J 18(4). ISSN 720–726:2215–986. https://doi.org/10.1016/j.jestch.2015.05.004
43. .Afzaal Ahmed (2016) Deposition and analysis of composite coating on aluminum using Ti–B4C powder Metallurgy tools in EDM. Mater Manuf Processes 31(4):467–474. https://doi.org/10.1080/10426914.2015.1025967
44. Papazoglou EL, Markopoulos AP, Papaefthymiou S, Manolakos DE (2019) Electrical discharge machining modeling by coupling thermal analysis with deformed geometry feature. J Adv Manuf Technol https://doi.org/10.1007/s00170-019-03850-8
45. Weingärtner E, Kuster F, Wegene, K (2012) Modeling and simulation of electrical discharge machining. In Procedia CIRP vol 2 74–78
46. Jahan MP (2015) Electrical discharge machining (EDM): types. Nova Science Publishers, Technologies and Applications
47. Mehta HN (2015) Modeling of electrical discharge machining process. Int J Eng Res Technol 4:153–156
48. Tlili A, Ghanem F, Salah NB (2015) A contribution in EDM simulation field. Int J Adv Manuf Technol 79:921–935
49. Vishwakarma UK, Dvivedi A, Kumar P (2012) FEA modeling of material removal rate in electrical discharge machining of Al6063/SiC composites. Int Conf Mech Ind Manuf Eng (ICMIME, 2012), Zurich, Switzerland, Jan. 15–17. 6, 586–591
50. Shabgard M, Ahmadi R, Seyedzavvar M, Oliaei SNB (2013) Mathematical and numerical modeling of the effect of input-parameters on the flushing efficiency of plasma channel in EDM process. Int J Mach Tools Manuf 65:79–87
51. Vignesh Shanmugam S, Krishnaraj V, Jagdeesh KA, Varun Kumar S, Subash S (2013) Numerical modelling of electro-discharge machining process using moving mesh feature. Procedia Eng 64:747–756
52. Papazoglou EL, Karmiris-Obratański P, Karkalos NE, Markopoulos AP (2020) On the use of deformed geometry in EDM modelling: Comparative study. Acta Physica Polonica A https://doi.org/10.12693/APhysPolA.138.268.
53. Liu JF, Guo YB (2016) Modeling of white layer formation in electric discharge machining (EDM) by incorporating massive random discharge characteristics. Procedia CIRP 42:697–702